Solution−Liquid−Solid Growth of Indium Phosphide Fibers from Organometallic Precursors: Elucidation of Molecular and Nonmolecular Components of the Pathway

Timothy J. Trentler,[†] Subhash C. Goel,[†] Kathleen M. Hickman,[†] Ann M. Viano,[‡] Michael Y. Chiang,[†] Alicia M. Beatty,[†] Patrick C. Gibbons,[‡] and William E. Buhro*,[†]

Contribution from the Departments of Chemistry and Physics, Washington University, St. Louis, Missouri 63130

Received November 25, 1996. Revised Manuscript Received January 2, 1997[⊗]

Abstract: Methanolysis of $\{t\text{-}Bu_2In[\mu\text{-}P(SiMe_3)_2]\}_2$ (**1**) in aromatic solvents gives polycrystalline InP fibers (dimensions 10−100 nm × 50−1000 nm) at 111−203 °C. The chemical pathway consists of a molecular component, in which precursor substituents are eliminated, and a nonmolecular component, in which the InP crystal lattices are assembled. The two components working in concert comprise the solution−liquid−solid (SLS) mechanism. The molecular component proceeds through a sequence of isolated and fully characterized intermediates: **1** → $[t\text{-}Bu_2In(\mu\text{-}OMe)]_2$ (**2**) → $[t\text{-}Bu_2In(\mu\text{-}PHSiMe_3)]_2$ (**3**) → **2** → $[t\text{-}Bu_2In(\mu\text{-}PH_2)]_3$ (**4**). Complex **4**, which is alternatively prepared from $t\text{-}Bu_3In$ and PH_3, undergoes alkane elimination, the last steps of which are catalyzed by the protic reagent MeOH, PhSH, Et_2NH, or $PhCO_2H$. In the subsequent nonmolecular component of the pathway, the resulting $(InP)_n$ fragments dissolve into a dispersion of molten In droplets, and recrystallize as the InP fibers. Important criteria are identified for crystal growth of covalent nonmolecular solids from (organic) solution. The outcomes of other solution-phase semiconductor syntheses are rationalized according to the functioning of molecular and nonmolecular pathway components of the kind identified here.

Introduction

Solution-phase organometallic syntheses of semiconductors are used for the growth of high-quality quantum dots,[1−3] and are potentially useful for the deposition of semiconductor materials on thermally sensitive substrates such as polymers or glasses. However, organometallic reactions that support the crystal growth of semiconductors or other covalent nonmolecular solids directly from solution are presently rare. We report the synthesis of crystalline InP from the solution-phase organometallic reaction 1a conducted at low temperatures. Our elucidation of the chemical pathway revealed unexpected factors responsible for InP formation and crystallization, prompting discovery of the solution−liquid−solid (SLS) crystal-growth mechanism.[4] The resulting insights enabled solution-phase synthesis of the crystalline III−V (13−15) compounds InP, InAs, and GaAs under comparably mild conditions from simpler organometallic precursors than were employed in eq 1.[4] Here we provide a full account of the conversion of the precursors $\{t\text{-}Bu_2In[\mu\text{-}P(SiMe_3)_2]\}_2$ (**1**, eq 1a) and $t\text{-}Bu_3In$ to polycrystalline InP fibers. This study identifies important mechanistic criteria for crystal growth of covalent nonmolecular solids from organometallic (or metalloorganic) precursors in solution.

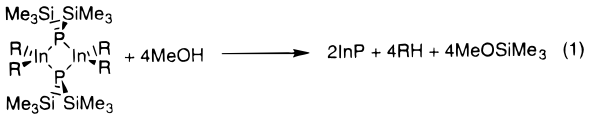

(a) R = *t*-Bu (**1**)
(b) R = CH_2SiMe_3
(c) R = CH_2-*t*-Bu

Molecular-precursor syntheses of semiconductors have been investigated since the 1960s.[5] Reactions conducted in solution yield three principal outcomes.[6] (1) Generally, elimination reactions precipitate incompletely converted molecular or oligomeric species containing the semiconductor elements *and* residual precursor substituents.[5,7−11] The reactions of trialkylgallanes or -indanes and phosphine or arsine are prototypical examples (eq 2).[5,7] (2) Some precursor-based syntheses precipitate the target semiconductors from solution, but in *amorphous* rather than crystalline form.[12−14] Examples are the alcoholyses of disilylphosphido and disilylarsenido precursors

[†]Department of Chemistry.
[‡]Department of Physics.
[⊗] Abstract published in *Advance ACS Abstracts,* February 1, 1997.

(1) Murray, C. B.; Norris, D. J.; Bawendi, M. G. *J. Am. Chem. Soc.* **1993**, *115*, 8706.
(2) Bowen Katari, J. E.; Colvin, V. L.; Alivisatos, A. P. *J. Phys. Chem.* **1994**, *98*, 4109.
(3) Micic, O. I.; Sprague, J. R.; Curtis, C. J.; Jones, K. M.; Machol, J. L.; Nozik, A. J.; Giessen, H.; Fluegel, B.; Mohs, G.; Peyghambarian, N. *J. Phys. Chem.* **1995**, *99*, 7754 and references therein.
(4) Trentler, T. J.; Hickman, K. M.; Goel, S. G.; Viano, A. M.; Gibbons, P. C.; Buhro, W. E. *Science* **1995**, *270*, 1791.
(5) (a) Didchenko, R.; Alix, J. E.; Toeniskoetter, R. H. *J. Inorg. Nucl. Chem.* **1960**, *14*, 35. (b) Harrison, B. C.; Tompkins, E. H. *Inorg. Chem.* **1962**, *1*, 951.
(6) Buhro, W. E. *Polyhedron* **1994**, *8*, 1131.
(7) Cowley, A. H.; Harris, P. R.; Jones, R. A.; Nunn, C. M. *Organometallics* **1991**, *10*, 652.
(8) (a) Wells, R. L.; Pitt, C. G.; McPhail, A. T.; Purdy, A. P.; Shafieezad, S.; Hallock, R. B. *Chem. Mater.* **1989**, *1*, 4. (b) Wells, R. L.; Self, M. F.; McPhail, A. T.; Aubuchon, S. R.; Woudenberg, R. C.; Jasinski, J. P. *Organometallics* **1993**, *12*, 2832. (c) Aubuchon, S. R.; McPhail, A. T.; Wells, R. L.; Giambra, J. A.; Bowser, J. R. *Chem. Mater.* **1994**, *6*, 82. (d) Wells, R. L.; Aubuchon, S. R.; Kher, S. S.; Lube, M. S.; White, P. S. *Chem. Mater.* **1995**, *7*, 793.
(9) Healy, M. D.; Laibinis, P. E.; Stupik, P. D.; Barron, A. R. *J. Chem. Soc., Chem. Commun.* **1989**, 359.
(10) Stuczynski, S. M.; Opila, R. L.; Marsh, P.; Brennan, J. G.; Steigerwald, M. L. *Chem. Mater.* **1991**, *3*, 379.
(11) (a) Matchett, M. A.; Viano, A. M.; Adolphi, N. L.; Stoddard, R. D.; Buhro, W. E.; Conradi, M. S.; Gibbons, P. C. *Chem. Mater.* **1992**, *4*, 508. (b) Goel, S. C.; Buhro, W. E.; Adolphi, N. L.; Conradi, M. S. *J. Organomet. Chem.* **1993**, *449*, 9.

S0002-7863(96)04085-1 CCC: $14.00

(eqs 1b,c, 3, and 4).[12,14] In some of these cases, the semiconductors are obtained as nanoparticles that may be too small to express regular crystal lattices. (3) As noted above, a few solution-phase organometallic (and metalloorganic) syntheses yield crystalline semiconductors directly. These include elimination reactions of the types shown in eqs 5 and 6, which are

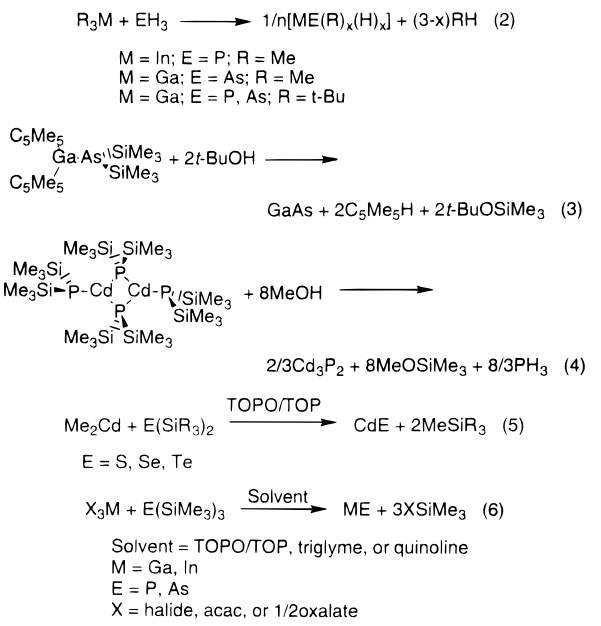

conducted in high-boiling coordinating solvents at >200 °C and produce semiconductor crystallites with dimensions of up to ca. 10 nm (100 Å).[1−3,15,16] Other cases, such as eq 1a, afford larger crystallites at lower solution temperatures.[4,17−19] We now present a rationale for the differing outcomes of solution-phase semiconductor syntheses, that is, for the extent of elimination achieved in solution and for the crystallinity (or noncrystallinity) of the resulting products.

The chemical pathway followed by eq 1a consists of two components: a molecular component comprising transformations of molecular intermediates, and a nonmolecular component comprising the steps in which the nonmolecular InP lattices are assembled. We show that elimination catalysis by protic reagants to generate $(InP)_n$ fragments is the critical aspect of the molecular component. To our knowledge, Theopold and co-workers were first to suggest such a role for protic reagents in organometallic reactions like eq 1.[12a] We further show that operation of the SLS mechanism[4] is the critical aspect of the nonmolecular component, which induces growth of polycrystalline InP fibers from a dispersion of nanometer-sized In metal droplets. Some of the results contained herein have been reported in preliminary form.[4,6]

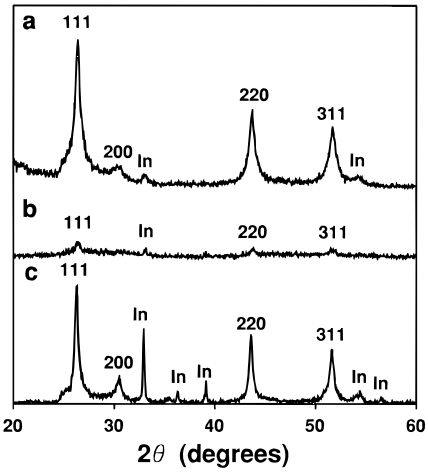

Figure 1. XRD Patterns: (a) eq 1a; (b) thermolysis of a solution of **4** at 111 °C in a heating mantle; (c) thermolysis of a solution of $[t\text{-}Bu_2In(\mu\text{-}PH_2)]_3$ (**4**) in the presence of MeOH catalyst (10 mol %) at 111 °C in a heating mantle. Peak intensities provide a qualitative estimation of the crystalline content in each sample.

Results

Growth of InP Fibers. Addition of methanol to toluene slurries of $\{t\text{-}Bu_2In[\mu\text{-}P(SiMe_3)_2]\}_2$ (**1**) gave colorless homogeneous solutions that yellowed slowly at room temperature, and became orange rapidly upon reflux. When refluxing was conducted in a *heating mantle* (see below), a black precipitate formed. Spectroscopic monitoring evidenced the clean generation of the molecular byproducts *t*-BuH (isobutane) and MeO-$SiMe_3$ (eq 1a). X-ray powder diffraction (XRD) established that the air-stable precipitate contained the crystalline phases InP (major) and metallic In (minor; Figure 1a). The crystalline coherence lengths calculated by the Scherrer equation were 9−16 and 28−71 nm for InP and In, respectively. Combustion analyses indicated retention of low levels of residual carbon (1.02%) and hydrogen (0.08%). This residue was likely traces of hydrocarbon solvents adsorbed onto the high-surface-area InP/In powder.

Transmission-electron-microscope (TEM) images showed the principal microstructural feature in the precipitate to be crooked fibers 10−100 nm in width and 50−1000 nm in length (Figure 2a,b). Energy dispersive X-ray spectroscopy conducted on individual fibers in the TEM gave 1:1 In:P ratios, within experimental limits. A wide-area (multiple-fiber) electron diffraction pattern (Figure 2c) gave diffraction rings that indexed to InP, with a slight apparent lattice contraction (observed, $a = 0.572$ nm; expected,[20] $a = 0.587$ nm), which was likely due to imperfect calibration of the TEM camera length rather than to a real contraction. The XRD data (Figure 1a) on the bulk sample showed no such contraction. The electron diffraction patterns of three individual fibers gave *a* values ranging from 0.570 to 0.579 nm. Thus, the fibers were identified as crystalline InP, the primary constituent of the bulk product.

Higher-resolution TEM lattice images revealed the polycrystallinity of the fibers. Numerous regions exhibiting corduroy patterns of ⟨111⟩ lattice fringes were evident. These regions formed a patchwork pattern of individual crystalline domains (grains), between which the lattice fringes were oriented in different directions. Unfortunately, the images were not of sufficient contrast for reproduction here. The domains appeared to have lateral dimensions of 10−20 nm, consistent with the average coherence length calculated from the line broadening in the XRD pattern (see above), and larger than the crystalline

(12) (a) Byrne, E. K.; Parkanyi, L.; Theopold, K. H. *Science* **1988**, *241*, 332. (b) Douglas, T.; Theopold, K. H. *Inorg. Chem.* **1991**, *30*, 594. (c) Douglas, T. Ph.D. Thesis, Cornell University, 1991.

(13) Stuczynski, S. M.; Brennan, J. G.; Steigerwald, M. L. *Inorg. Chem.* **1989**, *28*, 4431.

(14) Goel, S. C.; Chiang, M. Y.; Buhro, W. E. *J. Am. Chem. Soc.* **1990**, *112*, 5636.

(15) Olshavsky, M. A.; Goldstein, A. N.; Alivisatos, A. P. *J. Am. Chem. Soc.* **1990**, *112*, 9438.

(16) Uchida, H.; Matsunaga, T.; Yoneyama, H.; Sakata, T.; Mori, H.; Sasaki, T. *Chem. Mater.* **1993**, *5*, 716.

(17) Ramli, E.; Rauchfuss, T. B.; Stern, C. L. *J. Am. Chem. Soc.* **1990**, *112*, 4043.

(18) Hepp, A. F.; Andras, M. T.; Bailey, S. G.; Duraj, S. A. *Adv. Mater. Opt. Electron.* **1992**, *1*, 99.

(19) Brennan, J. G.; Siegrist, T.; Carroll, P. J.; Stuczynski, S. M.; Reynders, P.; Brus, L. E.; Steigerwald, M. L. *Chem. Mater.* **1990**, *2*, 403. In this study nanosized crystallites were produced, but at lower solution temperatures.

(20) West, A. R. *Solid State Chemistry and Its Applications*; Wiley: New York, 1984; p 237.

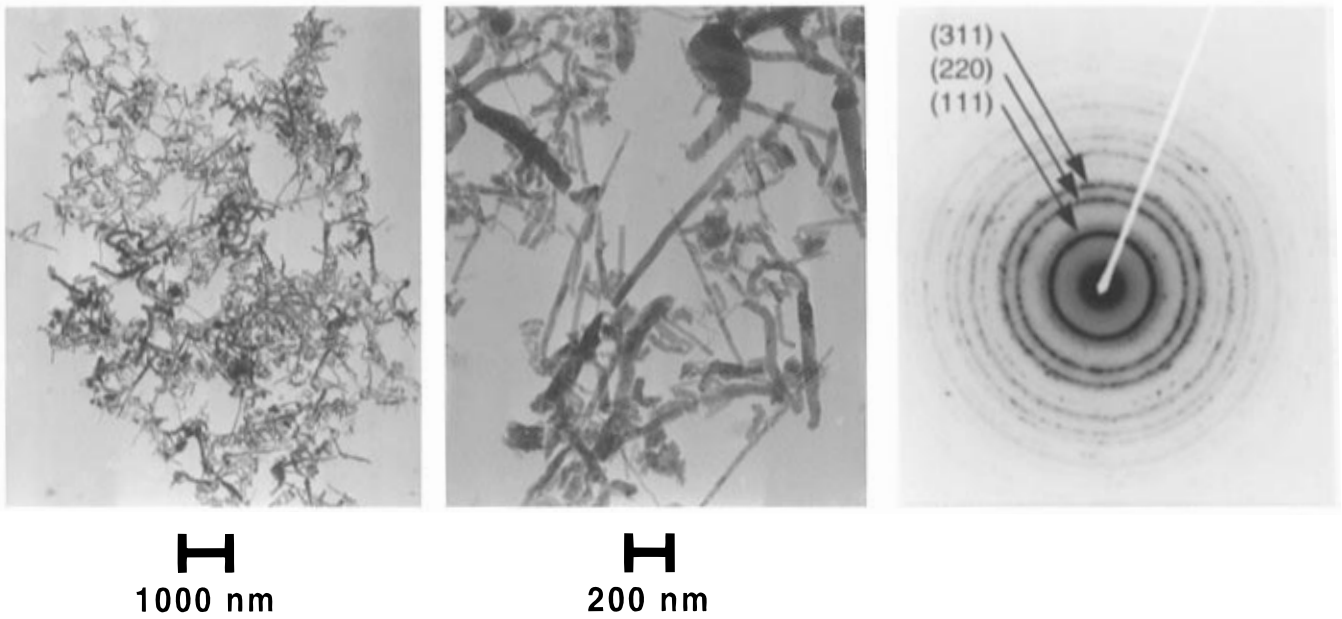

Figure 2. TEM data for InP fibers: (a, and b) dark-field images at two magnifications; (c) electron diffraction pattern. The indices refer to Bragg reflections in InP.

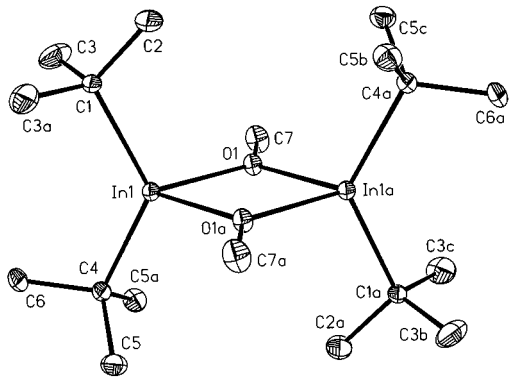

Figure 3. Thermal-ellipsoid plot of [*t*-$Bu_2In(\mu$-OMe)$]_2$ (**2**). Hydrogen atoms were omitted for clarity. Selected bond distances (Å): In(1)−O(1), 2.153(2); In(1)−O(1a), 2.153(2); In(1)−C(1), 2.188(6); In(1)−C(4), 2.191(5); O(1)−C(7), 1.398(4). Selected bond angles (deg): C(1)−In(1)−O(1), 109.0(1); C(1)−In(1)−O(1a), 109.0(1); O(1)−In(1)−O(1a), 75.2(1); C(4)−In(1)−O(1), 111.5(1); C(4)−In(1)−O(1a), 111.5(1); C(1)−In(1)−C(4), 128.2(1); In(1)−O(1)−In(1a), 104.8(1); In(1)−O(1)−C(7), 127.6(1); In(1a)−O(1)−C(7), 127.6(1).

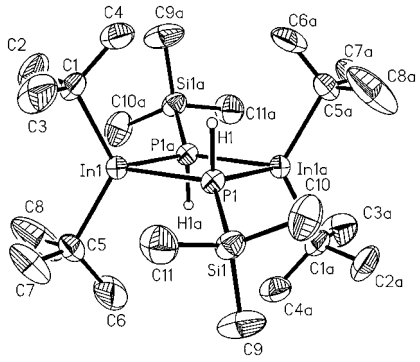

Figure 4. Thermal-ellipsoid plot of [*t*-$Bu_2In(\mu$-$PHSiMe_3)]_2$ (**3**). Hydrogen atoms were omitted for clarity. Selected bond distances (Å): In(1)−P(1), 2.683(1); In(1)−C(1), 2.190(5); In(1)−C(5), 2.198-(6); In(1)−P(1a), 2.637(1); P(1)−In(1a), 2.637(1); P(1)−Si(1), 2.239-(2). Selected bond angles (deg): P(1)−In(1)−C(1), 108.2(1); P(1)−In(1)−C(5), 112.9(1); C(1)−In(1)−C(5), 123.5(2); P(1)−In(1)−P(1a), 83.9(1); C(1)−In(1)−P(1a), 113.7(1); C(5)−In(1)−P(1a), 107.8(1); In-(1)−P(1)−In(1a) 96.1(1); In(1)−P(1)−Si(1), 127.7(1).

domain sizes obtained in other solution-based metalloorganic syntheses of III−V semiconductor crystallites.[3,8−10,12,15] Polycrystalline fibers, as opposed to single-crystal whiskers, are able to incorporate bends during growth, allowing the irregular, crooked fiber morphologies.

To our knowledge, the procedure summarized above and in eq 1a gave crystalline InP under the mildest known conditions. The unusual InP growth morphology, low growth temperature, and unprecedented solution-based growth conditions prompted us to determine the growth mechanism, as described below.

Elucidation of the Molecular Component of the Pathway. We observed and isolated three molecular intermediates on the eq 1a pathway between precursor **1** and InP, revealing two cycles of In−P bond cleavage and re-formation. Addition of MeOH to precursor **1** was expected to produce one or more of three initial outcomes: (1) methanolysis of In−C bonds to generate indium alkoxide species, (2) methanolysis of In−P bonds to generate indium-alkoxide species, or (3) methanolysis of P−Si bonds to generate new phosphidoindium species having P−H bonds. We establish below that the initial outcome of each methanolysis reaction was (2), and that subsequent steps produced the net outcome of (3).[12b,c] As described below, the last-detected, molecular intermediate was not unique to precursor **1**, and its *identity* did not account for the successful growth of crystalline InP. This result led to identification of a catalytic role for MeOH in the elimination steps that ultimately produced InP.

Two products were obtained from reactions of **1** and 2 molar equivalents of MeOH. After a short reaction time (2 min), the methoxide-bridged dimer [*t*-$Bu_2In(\mu$-OMe$)]_2$ (**2**) was isolated in 59% yield. The unexceptional structure of **2** is shown in Figure 3; it is isostructural to [*t*-$Bu_2Ga(\mu$-OMe$)]_2$[21] and similar to the previously determined structure of [*t*-$Bu_2In(\mu$-OEt$)]_2$.[22] After a longer reaction time (3 h), the phosphido-bridged dimer [*t*-$Bu_2In(\mu$-$PHSiMe_3)]_2$ (**3**) was isolated in 80% yield. Compound **3** was produced as an equal mixture of cis and trans isomers; the structure of the trans isomer is shown in Figure 4. Dialkylindane dimers like **3** possessing phosphido bridges are common, and Wells and co-workers have previously character-

(21) Cleaver, W. M.; Barron, A. R.; McGufey, A. R.; Bott, S. G. *Polyhedron* **1994**, *13*, 2831.
(22) Bradley, D. C.; Frigo, D. M.; Hursthouse, M. B.; Hussain, B. *Organometallics* **1988**, *7*, 1112.

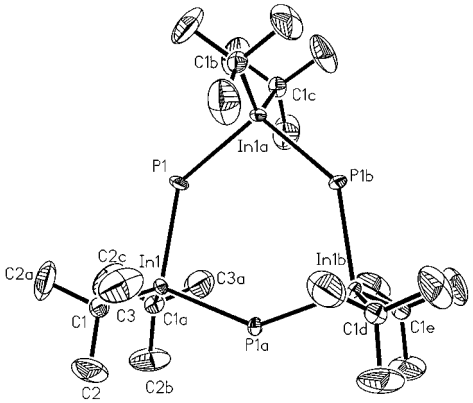

Figure 5. Thermal-ellipsoid plot of [*t*-$Bu_2In(\mu$-$PH_2)]_3$ (**4**). Hydrogen atoms were omitted for clarity. Selected bond distances (Å): In(1)−P(1), 2.627(3); In(1)−P(1a), 2.627(6); P(1)−In(1a), 2.627(3); In(1)−C(1), 2.200(15); In(1)−C(1a), 2.200(15). Selected angles (deg): P(1)−In(1)−C(1), 106.6(2); P(1)−In(1)−P(1a), 101.2(3); C(1)−In(1)−P(1a), 106.6(2); P(1)−In(1)−C(1a), 106.6(2); C(1)−In(1)−C(1a), 126.7(8).

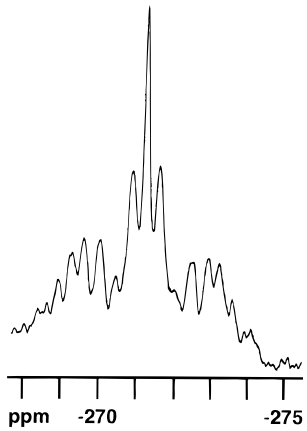

Figure 6. ^{1}H-coupled ^{31}P NMR spectrum of [*t*-$Bu_2In(\mu$-$PH_2)]_3$ (**4**).

ized such a derivative containing a μ-$PHSiMe_3$ ligand.[23] Spectroscopic monitoring established that **2** and **3** were formed by the sequential reactions in eqs 7 and 8. Thus, the In−P bonds in **1** were initially cleaved by methanolysis, and were subsequently re-formed.

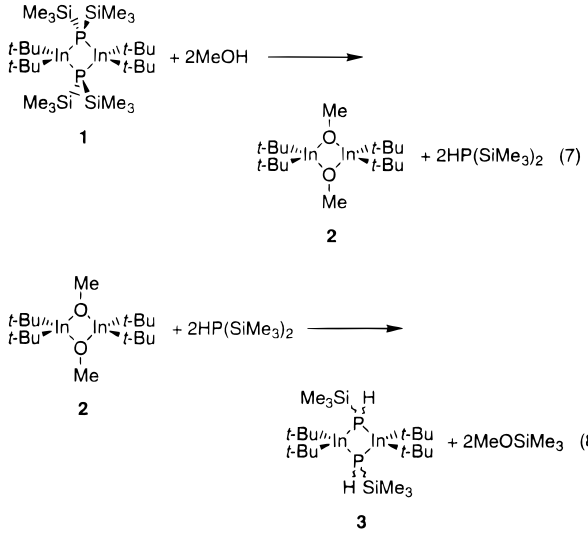

As in the case for **1** just described, two products were obtained from reactions of **3** and 2 molar equivalents of MeOH. At short reaction times (ca. 2 min) significant amounts of the methoxide **2** were observed to form by spectroscopic monitoring. After longer reaction times (3 h) the trimer [*t*-$Bu_2In(\mu$-$PH_2)]_3$ (**4**) was isolated in 53% yield. The structure of **4** is shown in Figure 5; **4** is isomorphous and isostructural to [*t*-$Bu_2Ga(\mu$-$PH_2)]_3$, which was prepared and characterized by Cowley, Jones, and co-workers.[7] Like [*t*-$Bu_2Ga(\mu$-$PH_2)]_3$,[7] **4** has a characteristically complex proton-coupled ^{31}P NMR spectrum (see Figure 6). Spectroscopic monitoring established that **2** and **4** were formed by the sequential reactions in eqs 9 and 10. Thus, precursor **1** was converted to trimer **4** by the eqs 7−10 sequence, comprising two cycles of In−P bond cleavage and re-formation.

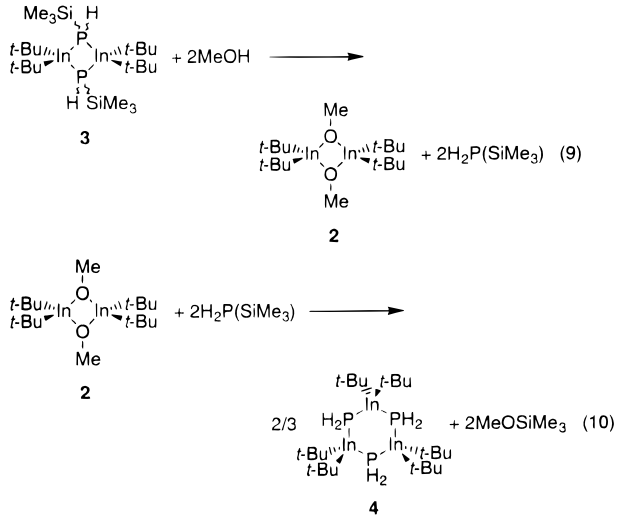

We found that **4** was generated directly from *t*-Bu_3In and PH_3 (eq 11), by analogy to the synthesis of [*t*-$Bu_2Ga(\mu$-$PH_2)]_3$ reported by Cowley, Jones, and co-workers.[7] Precursor **1** was

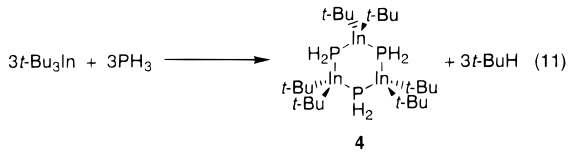

also prepared from *t*-Bu_3In (see the Experimental Section). The direct production of **4** by eq 11 constitutes a savings of at least two procedures over its preparation via **1** and eqs 7−10.

Methanolysis product **4** was observed to form during spectroscopic monitoring of eq 1a, and was the last isolable or detectable, discrete, molecular intermediate on the pathway. However, isolated or independently generated (eq 11) **4** did *not* yield crystalline InP by simple thermal decomposition at the temperatures used in eq 1a. Gradual decomposition of **4** ensued immediately in room-temperature solutions, as evidenced by the generation of isobutane (*t*-BuH) and the appearance of a very broad ^{31}P{^{1}H} NMR resonance (−230 to −260 ppm) that we assigned to complex In−P oligomers. When these solutions were refluxed at 111 °C, the resulting precipitates retained significant quantities of residual alkyl substituents, and analyzed for the approximate empirical formula [(*t*-$Bu)_{0.30}InPH_{0.30}$]. The XRD patterns contained broad, amorphous features punctuated by sharper, low- to moderate-intensity reflections for InP, indicating varying amounts of a crystalline fraction (coherence length ≤12 nm) within a primarily noncrystalline product (see Figure 1b).

Solution thermolysis of **4** at 203 °C produced InP of comparable purity and crystallinity to that obtained from eq 1a. Residual carbon and hydrogen were reduced to near the levels observed in eq 1a, and the average crystalline coherence length in the InP product (9 nm) was within the range achieved in eq 1a. Thus, the production of crystalline InP by thermal decom-

(23) Wells, R. L.; McPhail, A. T.; Self, M. F. *Organometallics* **1993**, *12*, 3363 and references therein.

Table 1. Survey of Catalysts for Conversion of **4** to InP (Eq 12)

catalyst	solution temp (°C)	heating method[a]	InP coherence length (nm)	InP Anal. (% C, % H, % N)[b]	InP yield (%)[c]
none	111	M	≤2	9.90, 1.39, 0.00	0[d]
$PhCO_2H$	111	M	18	1.43, 0.05, 0.00	42
PhSH	111	M	11	1.95, 0.18, 0.00	78
H_2O	111	M	≤2		0
MeOH	111	M	10	1.04, 0.10, 0.00	70
t-BuOH	111	M	≤2		0
Et_2NH	111	M	16	0.79, 0.02, 0.00	69
Et_3N	111	M	≤2	12.53, 2.36, 0.09	0
$PhCO_2H$	111	O	≤2	12.42, 1.88, 0.00	0
PhSH	111	O	≤2	10.56, 1.48, 0.00	0
MeOH	111	O	≤2	12.24, 1.15, 0.00	0
none	203	O	9	1.24, 0.14, 0.00	88
PhSH	203	M	25		77
MeOH	203	M	9		71
MeOH	203	O	9		86

[a] M = heating mantle; O = oil bath. [b] Average values of multiple analyses. [c] Yields were calculated by dividing the mass of the InP/In product by the theoretical mass of InP (assuming complete conversion of indane precursor to InP). [d] Yields of crystalline InP were assumed to be zero in products having small mean coherence lengths (≤2 nm).

position of **4** required solution temperatures considerably higher than those used in eq 1a (111 °C).

The failure of isolated or independently generated (eq 11) **4** to produce wholly crystalline InP from solution at 111 °C was consistent with ample precedent. As stated in the Introduction, solution-phase reactions of trialkylindanes or -gallanes and phosphine or arsine have not produced crystalline semiconductors (see eq 2).[5,7] Trimer **4** was an intermediate in such a reaction (see eq 11). Obviously a condition (or conditions) present during decomposition of **4** in eq 1a was not reproduced in the direct thermal decomposition of isolated or independently generated **4**.

The missing condition was the presence of MeOH. In eq 1a, **4** was generated and decomposed in a mixture containing at least traces of MeOH. When independently synthesized **4** was heated at 111 °C with a catalytic amount (10 mol %) of MeOH, crystalline InP was obtained as in eq 1a. Residual carbon and hydrogen levels in the product were low, and the XRD pattern was sharp (see Figure 1c; coherence length 10 nm). We surmised that MeOH catalyzed the elimination reaction in eq 12. The variable crystalline fractions produced

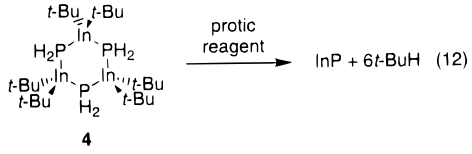

4

protic reagent → InP + 6*t*-BuH (12)

at 111 °C in the absence of MeOH were presumably due to adventitious catalysis by trace protic impurities.

We then surveyed a series of other potential catalysts (Table 1). Intermediate **4** was generated by eq 11, and 0.1 molar equivalent (based on *t*-Bu_3In) of the potential catalysts was added. As shown in Table 1, H_2O, *t*-BuOH, and NEt_3 were ineffective for promoting eq 12. The compounds $PhCO_2H$, PhSH, MeOH, and NEt_2H *were* effective, and yielded coherence lengths of 10−18 nm at 111 °C when mantle heating was employed. Note that the effective catalysts were protic reagents with pK_a values over a wide range (4−36); we concluded that the alkane-elimination steps contained within eq 12 were weak-acid-catalyzed. Catalyst performance as indicated by InP yield, purity, or coherence length was not evidently correlated with catalyst pK_a. A mechanistic rationale is given in the Discussion.

Complete alkane elimination is a necessary but insufficient condition for InP crystal growth. Effective catalysts decreased the temperature at which complete elimination was achieved, enabling crystal growth as long as other necessary conditions were met. Thus, eqs 7−10 and 12 constituted the molecular component of the eq 1a pathway. Presumably, InP was generated initially from eq 12 as *noncrystalline* $(InP)_n$ clusters or fragments, because the insolubility of InP in conventional solvents precludes direct, solvent-phase assembly of the regular InP crystal lattice (see the Discussion).[4] The molecular component provided the nutrient species for the crystal-growth process, which occurred in the nonmolecular component of the eq 1a pathway as established below.

Elucidation of the Nonmolecular Component of the Pathway. As previously noted, some metallic In always formed as a side product with crystalline InP in eq 1a. A series of observations established a critical role for In metal in InP crystallization. Organometallic analogs to **1** or to *t*-Bu_3In that failed to produce In as a byproduct also failed to give crystalline InP. TEM studies revealed frozen, nanometer-sized In droplets attached to the ends of polycrystalline InP fibers; our results indicated that these In droplets were the sites from which the InP fibers grew. Mechanistic studies verified that the polycrystalline fibers grew only under conditions in which the In droplets were molten (liquid), and confirmed that elemental phosphorus had sufficient solubility in molten In at temperatures below 200 °C to generate crystalline InP. The combined results indicated a three-phase SLS[4] crystal-growth pathway in which solution-phase reactions supplied In and P to the liquid In droplets, which became supersaturated, precipitating solid (polycrystalline) InP. In this manner, a covalent nonmolecular solid was crystallized in conjunction with organometallic reactions conducted in solution. The details supporting the proposed nonmolecular component of the eq 1a pathway are given below.

The ability of several organoindanes to produce crystalline InP under conditions comparable to eq 1a was evaluated. The methanolysis of $\{Me_2In[\mu\text{-}P(SiMe_3)_2]\}_2$, the methyl homolog of precursor **1**, gave amorphous material containing large amounts of residual C and H. Douglas and Theopold previously reported that methanolysis of the (trimethylsilyl)methyl and neopentyl homologs of **1** gave amorphous and/or nanoparticulate InP by eq 1.[12b,c] None of these, except the reaction of **1**, produced In metal in amounts detectable by XRD. Among this homologous series of compounds, **1** was unique in producing In metal, and in producing crystalline InP.

We also examined reactions between PH_3 and aryl and alkyl analogs to *t*-Bu_3In under conditions comparable to the eqs 11 and 12 sequence. These experiments were undertaken to establish the dependence of reaction pathway on the In substituent, and to possibly identify an alternative precursor to *t*-Bu_3In, which is somewhat difficult to prepare and decomposes gradually upon long-term storage.[22] The compounds $(2,4,6\text{-}Me_3C_6H_2)_3In$ and PH_3 were allowed to react at 111 °C with a catalytic amount of MeOH. The compounds Et_3In and PH_3 were allowed to react at 203 °C without a protic catalyst. In both cases amorphous material was produced having an XRD pattern similar to that in Figure 1b, rather than crystalline InP. In neither case was In metal detected by XRD.

In contrast to the above, $(Me_2EtC)_3In$ and PH_3 gave crystalline InP (coherence length 10 nm) at 203 °C without a protic catalyst; In metal was *also* formed in this reaction. Thus, each time crystalline InP was obtained in the present work, so was In metal. Bradley and co-workers reported that *t*-Bu_3In and other *t*-Bu-substituted indanes decomposed photochemically (in daylight) to indium metal, isobutane, and isobutene among other products.[22] We found that *t*-Bu_3In and $(Me_2EtC)_3In$ were also *thermally* unstable in solution to give In metal, unlike the

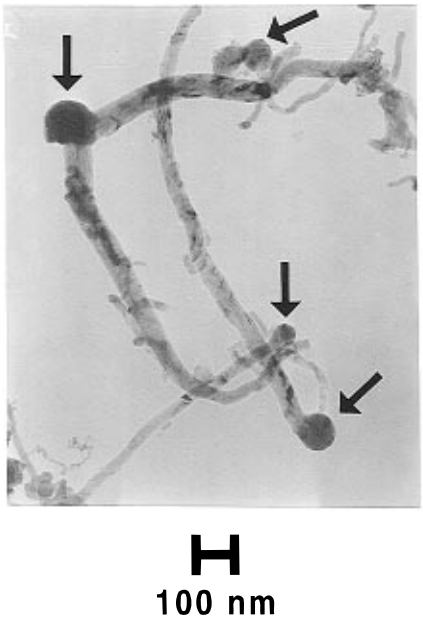

Figure 7. TEM image of InP fibers showing In spherules (arrows) at fiber tips.

indanes lacking tertiary alkyl substituents. Therefore, the source of metallic In in eq 1a and related procedures was likely thermal decomposition of **4** or other tertiary-alkyl-containing intermediates.

The intermediates derived from reaction of Et_3In and PH_3 lacked tertiary alkyls, were consequently stable with respect to In formation, and produced amorphous products (see above). We repeated the experiment by adding PhSH as a protic catalyst and *t*-Bu_3In as an In source *after* the initial reaction between Et_3In and PH_3. The mixture produced both crystalline InP (coherence length 7 nm) *and* metallic In at 203 °C. Thus, metallic In was strongly implicated in the InP crystal-growth process.

The distribution of In in the TEM images of the InP samples was expected to provide clues about the role of In. Note that metallic In was not evident in the Figure 2 images although metallic In was certainly present in the sample. Under normal TEM operating conditions, In was readily melted under the electron beam and splattered out of the field of view.

Undisturbed In metal was successfully imaged at a lower e-beam current density. Indium spherules were often found affixed to the ends of isolated InP fibers (see Figure 7). Metallic In was also found in other configurations. Fibers often formed porous, tangled bundles having their fiber tips soldered together at numerous In vertices within the bundles. When the e-beam current density was increased, the spherules melted and some InP fibers dissolved into growing pools of liquid In (see below). This principal microstructural feature—spherulitic In particles having one or more InP fiber tips embedded into them—was the key indicator of the crystal-growth mechanism.

The In spherules (droplets) were strongly implicated as the crystallization medium for growth of InP by the SLS mechanism. The distinguishing features of SLS growth are (1) a solution dispersion of small liquid flux droplets, (2) a solution phase that feeds the elements of the crystal phase into the flux droplets, and (3) pseudo-one-dimensional growth of the crystal phase from the flux droplets after supersaturation is achieved (see Figure 8).[4] The SLS mechanism is closely analogous[4] to the well-known vapor−liquid−solid (VLS) mechanism,[24] in

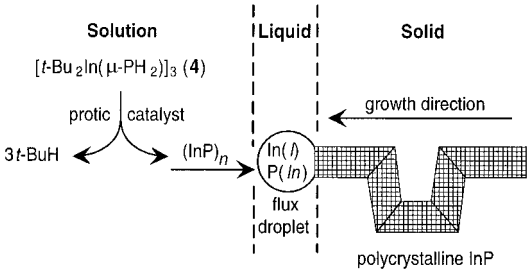

Figure 8. Solution−liquid−solid (SLS) crystal-growth mechanism.

which whisker crystals are grown from flux droplets that are fed from the vapor phase rather than a solution phase. Retro-VLS, or SLV, processes are also known, in which crystals are *consumed* by flux droplets and their constituent elements liberated to the vapor phase.[25] An SLV mechanism was operating during TEM examination of our fibers at higher e-beam current densities, where they redissolved into liquid In with the release of volatile P_4 (or P_2) vapor to the high-vacuum TEM environment (see above). That is, the reverse of the proposed *crystal-growth* (nonmolecular) process was directly observed in real time. Thus, liquid In served as a flux for InP crystal growth or crystal decomposition when in contact with an appropriate solution phase or vacuum.

To verify the proposed role of In, we sought to demonstrate that it was indeed molten under our reaction conditions. The normal melting point of In is 157 °C, and In is not known to form a (lower-melting) eutectic by dissolution of P.[26] Consequently, reaction temperatures above 157 °C should have been required to produce crystalline InP by the proposed SLS mechanism. As stated above, crystalline InP was obtained from reactions conducted in refluxing toluene (111 °C), provided that a heating mantle was employed. In those experiments we found significant amounts of the black In/InP product adhering to the walls of the reaction vessels. When the heating mantle was replaced by an oil bath held at approximately 145 °C, the reactions failed to produce crystalline InP. When the reaction was conducted in refluxing mesitylene (1,3,5-$Me_3C_6H_3$, bp 164 °C) in a 170 °C oil bath, crystalline InP was again produced. These results suggested strongly that molten In was necessary for InP crystal growth.

We inferred that mantle heating produced a larger thermal gradient at the walls of the glass reaction vessels than did oil-bath heating, and that temperatures ≥157 °C were required in either case. As stated above, oil-bath temperatures slightly above the In melting point gave crystalline InP whereas oil-bath temperatures below the In melting point did not. With mantle heating, In nanoparticles collecting on the vessel walls apparently experienced hot-spot temperatures above 157 °C, even in refluxing toluene (bp 111 °C).

Finally, we sought to confirm that P was sufficiently soluble in liquid In at our reaction temperatures to support InP crystal growth. Phosphorus is only minimally soluble in liquid In; extrapolation of thermodynamic data collected at higher temperatures[26] indicates that the equilibrium atomic fraction of P in a saturated In(l) solution is $\sim 10^{-8}$ at temperatures below 200 °C. To establish if this low solubility was consistent with InP crystallization in quantities and at rates comparable to those achieved in eq 1a, we studied the direct reaction of liquid In and P_4 under comparable conditions. A dispersion of submicrometer-sized In droplets was prepared by high-intensity sonication of In at 164 °C in mesitylene. A P_4 solution was

(24) (a) Wagner, R. S. In *Whisker Technology*; Levitt, A. P., Ed.; Wiley: New York, 1970; Chapter 3. (b) Givargizov, E. I. In *Current Topics in Materials Science*; Kaldis, E., Ed.; North-Holland: Amsterdam, 1978; Vol. 1, Chapter 3.

(25) Retro-VLS or SLV processes are also referred to as "negative whisker growth". (a) Wagner, R. S. *J. Cryst. Growth* **1968**, *3*−4, 159. (b) Schoonmaker, R. C.; Buhl, A.; Lemley, J. *J. Phys. Chem.* **1965**, *69*, 3455.

(26) Kuphal, E. *J. Cryst. Growth* **1984**, *67*, 441.

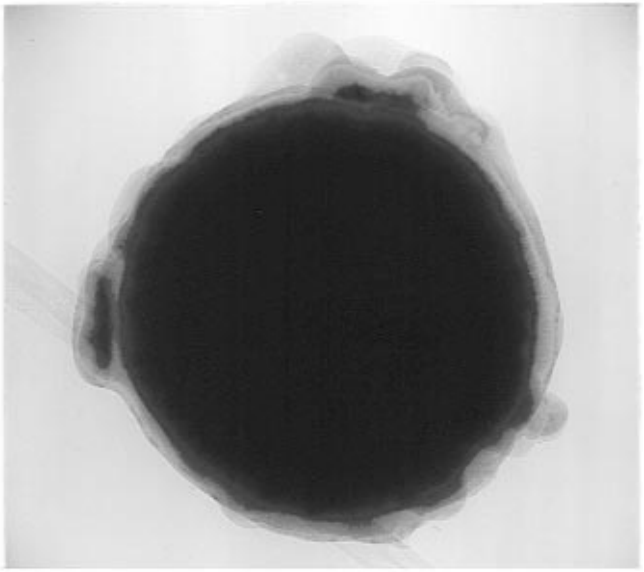

Figure 9. Representative In spherule coated with InP crystallites generated by reaction of an In dispersion with P_4. The dark central region is In; the lighter, irregular periphery is crystalline InP.

added to the hot In dispersion, which darkened immediately with the conversion of a significant fraction of the In to crystalline InP as confirmed by XRD (InP coherence length 50 nm). A TEM image revealed In spherules coated with InP crystallites (Figure 9), strongly suggesting that P had dissolved into the droplets and InP had subsequently crystallized out at the droplet surfaces. Indium dispersions and P_4 did not react at temperatures below the melting point of In. The solubility of P in liquid In under our reaction conditions was thus sufficient for InP crystal growth at readily observable rates, supporting the proposed SLS mechanism.

We concluded that the InP crystal lattices were assembled in a nonmolecular component of the eq 1a pathway that comprised crystal-growth steps operating in conjunction with the previously described molecular (ligand-elimination) component of the pathway. Liquid In as small flux droplets was the true crystal-growth solvent. The SLS growth mechanism coordinated the dynamics of three phases in intimate contact—the organometallic reaction solution, the In crystallization liquid, and the growing InP solid fibers.

Discussion

Requirements for Crystal Growth. As detailed elsewhere,[4,27] one of two conditions must exist for uniform crystal-lattice construction to occur. Adspecies from a fluid nutrient phase (vapor, melt, or solution) must either be capable of reversible adsorption−desorption from a crystal-growth surface or have rapid diffusional mobility upon a growth surface. These conditions allow mispositioned adspecies to find proper sites in growing crystals.

Neither crystal-growth condition typically exists in solution-phase semiconductor syntheses. The elimination reactions used to deposit semiconductor elements are generally chemically irreversible (eqs 1−6), and no soluble species are generally desorbable from semiconductor growth surfaces. The cascades of covalent-bond-making and -breaking events necessary to support atomic surface diffusion are energetically precluded at the low temperatures typically employed in solution-phase chemistry. We have argued that the observed growth of nearly defect-free semiconductor nanocrystals at higher temperatures in coordinating solvents[1−3] is allowed by a special occurrence of solid-state diffusional mobility that disappears with increasing crystallite size.[27] Crystalline domains as large as were observed in this study should not be directly accessible by low-temperature solution chemistry. Indeed, crystal growth under our conditions occurs only *indirectly* from the organic-solvent phase through the intervention of a liquid-metal crystallization phase, a special provision in the SLS pathway.

Scheme 1. Direct Intermolecular Elimination−Condensation of $[t\text{-Bu}_2\text{In}(\mu\text{-PH}_2)]_3$ (**4**) to a Zinc-Blende Cluster Fragment[a]

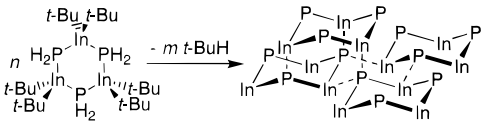

4

[a] Peripheral *t*-Bu and H cluster substituents are omitted for clarity. The dotted lines are bonds formed by intermolecular elimination; the solid lines are bonds preexisting in **4**.

The SLS mechanism provides a novel means for activating reversible adspecies adsorption−desorption and likely also surface diffusional mobility at low solution temperatures. As indicated above, these processes are inactive at liquid−solid interfaces between semiconductor crystals and reaction solutions in conventional organic solvents. However, such processes do operate, presumably with monoatomic In and P solutes and adspecies, at the liquid−solid interface between an In flux droplet and an InP crystallite (Figure 8). This allows SLS InP growth to proceed in organic-solvent dispersions at temperatures considerably below those required by organometallic chemical vapor deposition (≥500 °C, surface diffusion)[28] or melt crystallization (≥1000 °C, surface diffusion and/or adsorption−desorption).[29]

Role of Protic Catalyst. As stated above, solution-phase reactions of R_3In or R_3Ga and PH_3 or AsH_3 typically do not afford complete elimination to the binary semiconductor (eq 2). We found that *t*-Bu_3In and PH_3 gave, at 111 °C without a catalyst, a product corresponding to elimination of ∼2.70 of the expected 3.00 equiv of *t*-BuH. Apparently, the protic catalyst is required for promoting elimination of the last ∼0.30 equiv. Our proposed elimination−condensation model below accounts for the difficulty in liberating the last small amounts of alkane, and the role of the catalyst in assisting it.

In the eq 12 elimination−condensation process, *t*-BuH elimination is coupled with In−P bond formation, bringing about the oligomerization (condensation) of molecular intermediates. The resulting cluster fragments should likely adopt core structures resembling the stable, zinc-blende structure of crystalline InP.[30] Because the six-membered metallacycle **4** is the last-detected molecular intermediate, one may propose that *t*-BuH elimination proceeds by direct intermolecular condensation of **4** (Scheme 1). As shown in Scheme 1, condensation of chairlike In_3P_3 rings can produce zinc-blende fragments. A similar condensation process has been proposed by Gladfelter and co-

(27) Buhro, W. E.; Hickman, K. M.; Trentler, T. J. *Adv. Mater.* **1996**, *8*, 685.

(28) Ludowise, M. J. *J. Appl. Phys.* **1985**, *58*, R31.

(29) Dugue, M.; Goullin, J. F.; Merenda, P.; Moulin, M. In *Preparative Methods in Solid State Chemistry*; Hagenmuller, P., Ed.; Academic: New York, 1972; pp 309−360.

(30) (a) Dance, I. G.; Choy, A.; Scudder, M. L. *J. Am. Chem. Soc.* **1984**, *106*, 6285. (b) Herron, N.; Calabrese, J. C.; Farneth, W. E.; Wang, Y. *Science* **1993**, *259*, 1426. (c) Vossmeyer, T.; Reck, G.; Katsikas, L.; Haupt, E. T. K.; Schulz, B.; Weller, H. *Science* **1995**, *267*, 1476. (d) Vossmeyer, T.; Reck, G.; Schulz, B.; Katsikas, L.; Weller, H. *J. Am. Chem. Soc.* **1995**, *117*, 12881.

Scheme 2. Proposed Catalytic Cycle for Stereochemically Disfavored Elimination−Condensation Steps[a]

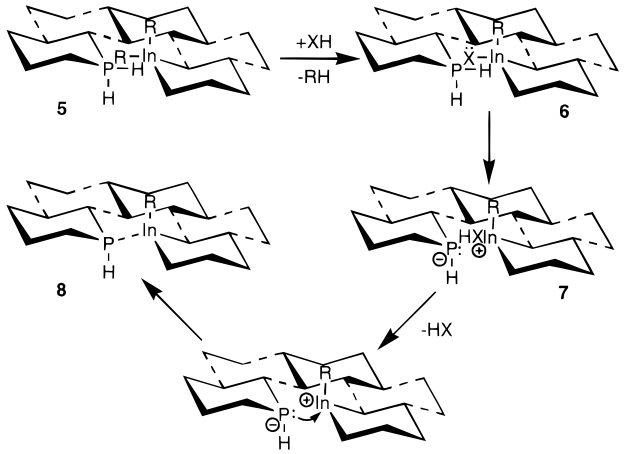

[a] The cycle (step) is depicted for a hexagonal-net fragment derived from [*t*-$Bu_2In(\mu$-$PH_2)]_3$ (**4**); solid lines represent bonds preexisting in molecules of **4**. Only the participating In and P centers are labeled; other atom labels and peripheral substituents are omitted for clarity.

workers to account for conversion of the six-membered cyclotrigallazane $[H_2GaNH_2]_3$ to the wurtzitic GaN.[31]

Initially, intermolecular elimination−condensation of **4** should occur readily, because conformationally mobile metallacycles should easily achieve the mutual orientations necessary for four-center elimination of *t*-BuH. Indeed, elimination−condensation *begins* in solution even at room temperature, and in the absence of added protic catalysts (or In particles; see above).

However, as elimination−condensation proceeds and the conformational rigidity of the resulting fragments increases, situations arise for which four-center elimination is highly disfavored. For example, structure **5** (Scheme 2) depicts a hexagonal-net fragment resulting from condensation of five molecules of **4.** Note that in **5** the depicted In and P centers have an incorrect regiochemistry for a four-center elimination to give an In−P bond; the In and P atoms are anti rather than syn in the four-center arrangement. These and related situations should arise whether elimination−condensation occurs by the straightforward intermolecular condensation of **4** as suggested in Scheme 1, or by a more complex pathway. We propose that protic catalysis is particularly vital for promoting elimination steps that, as in **5**, cannot proceed by a direct four-center process. Such elimination steps likely correspond to a significant component of the last ∼0.30 equiv of *t*-BuH in eq 12.

Protolytic cleavage of a *t*-Bu−In bond by a catalyst XH is the first step in our proposed catalytic cycle (see Scheme 2). The catalysts we identified are sufficiently reactive to cleave indium−alkyl bonds with attendant In−X bond formation,[32] generating intermediates like **6**. Proton transfer from P to a lone pair on X, perhaps with intermolecular participation of a second molecule of XH, produces a zwitterion with a good leaving group (**7**). Loss of XH followed by collapse of the zwitterion regenerates the protic catalyst and forms the In−P bond (**8**).

Schwartz and co-workers studied metalloorganic reactions on hydroxylated surfaces that are relevant to Scheme 2.[33] They found that proton transfer from a surface hydroxyl to a surface-bound $Zr(O$-*t*-$Bu)_4$ is more rapid than to a surface-bound $Zr(CH_2$-*t*-$Bu)_4$ (within the conformationally restricted surface environment), despite the stronger thermodynamic driving force for the latter. This was attributed to the kinetic facility of proton transfer to an O (X) lone pair relative to a metal−alkyl σ bond in the surface-confined reaction environment. Likewise, we assert that the proton transfer to X in **6** as depicted in Scheme 2 should be considerably faster than a corresponding proton transfer to R in **5**. Thus, conformationally disfavored alkane eliminations may be catalyzed by appropriate protic reagents.

We believe that the crucial last steps of catalyzed alkane elimination occur at the interface between the reaction solution and the In flux droplet (see Figure 8). Indeed, when intermediate **4** was decomposed (eq 12) at 111 °C in an oil bath in the presence of the protic catalysts, but in the *absence* of In droplets, alkane elimination was incomplete (see Table 1). This suggests that catalysis must occur upon the surface of the In droplets, at least for the final elimination steps.

The molecular, elimination−condensation pathway we have proposed may possibly generate *large*, zinc-blende cluster fragments, but would be incapable of producing the extended structural periodicity (crystallinity) and the large InP fiber dimensions for the reasons given in Requirements for Crystal Growth (see above). The cluster fragments should have external faces terminated by residual In−*t*-Bu and P−H groups. Elimination of these last *t*-Bu and H substituents should be completed on the flux-droplet surfaces so that the resulting naked $(InP)_n$ clusters may immediately dissolve (presumably with dissociation) into the metallic flux. Naked $(InP)_n$ clusters could have only a short lifetime in solution (in a noncoordinating solvent) prior to agglomeration and precipitation as amorphous solid. That crystalline InP was obtained suggests that naked $(InP)_n$ clusters are generated in close proximity to (or *on*) the In flux droplets. Once In and P are deposited into the flux the nonmolecular component of the pathway, described above, assembles the polycrystalline fibers.

Rationale for Outcomes of Solution-Phase Semiconductor Syntheses. The three outcomes of metalloorganic semiconductor syntheses noted in the Introduction are (1) incomplete elimination, (2) production of an amorphous semiconductor, and (3) production of a crystalline semiconductor. These outcomes are given in order of decreasing frequency and increasing importance. No preexisting rationale accounts for the outcome achieved by any specific synthesis.

We propose that the outcome depends on the functioning of molecular and nonmolecular pathway components of the kind identified here. To produce crystalline material, both components must function effectively. If the molecular component operates but the nonmolecular component does not, then amorphous material is produced; precursor substituents are eliminated completely, but no means exist for assembling the nonmolecular crystal lattices. If the molecular component fails, then incomplete elimination obtains.

In a recent review we analyzed organometallic syntheses represented by eqs 1 and 2, finding many mechanistic similarities between them.[6] Despite these similarities, the reactions give consistently different outcomes, which were inexplicable when the review was written. We now understand that reactions corresponding to eq 2 give incomplete elimination for lack of an elimination catalyst and the consequent inefficiency of the molecular component of the pathway. Reactions corresponding to eq 1 generally give amorphous or nanoparticulate materials because a protic catalyst is present and the molecular component is successful. When the eq 1 precursor contains *t*-Bu substituents some metallic In forms during the reaction, activating the nonmolecular component of the pathway and producing crystalline InP. We propose that all organometallic (or metalloorganic)

(31) Hwang, J.-W.; Campbell, J. P.; Kozubowski, J.; Hanson, S. A.; Evans, J. F.; Gladfelter, W. L. *Chem. Mater.* **1995**, *7*, 517.

(32) Tuck, D. G. In *Comprehensive Organometallic Chemistry*; Wilkinson, G.; Stone, F. G. A., Abel, E. W., Eds.; Pergamon: Oxford, 1982; Vol. 1, Chapter 7, p 711.

(33) Miller, J. B.; Schwartz, J.; Bernasek, S. L. *J. Am. Chem. Soc.* **1993**, *115*, 8239.

semiconductor syntheses conducted in solution at low temperatures may now be similarly rationalized. The outcomes depend on the success or failure of (1) molecular pathways for elimination−condensation (possibly catalyzed) *and* (2) nonmolecular pathways for assembling the covalent crystal lattices.

Conclusion

Low-temperature, solution-based growth of crystalline InP proceeds by the SLS pathway, which comprises an effective substituent-elimination mechanism working in concert with an effective crystallization mechanism. These are the necessary and sufficient conditions for organometallic synthesis of crystalline covalent nonmolecular solids under *any* conditions (including those for CVD). The key to reducing growth temperatures is identifying novel crystal-growth pathways that function at lower temperatures. Further developments in this area may bring the synthesis of nonmolecular inorganic materials into the regime of conventional, solution-phase organometallic chemistry.

Experimental Section

General Methods. All ambient-pressure procedures were carried out under dry N_2 using standard inert-atmosphere techniques. *t*-Bu_3In,[22] $(Me_2EtC)_3In$,[34] and $(2,4,6\text{-}Me_3C_6H_2)_3In$[35] were prepared by the procedures of Bradley and Barron. Et_3In was used as received from Strem. $\{t\text{-}Bu_2In[\mu\text{-}P(SiMe_3)_2]\}_2$ (**1**) was prepared as a white precipitate from *t*-Bu_3In and $HP(SiMe_3)_2$[36] in hexane. $^{31}P\{H\}$ NMR (ppm, benzene-d_6): −189.3 (s). Mp: 152−3 °C dec.[37] $\{Me_2In[\mu\text{-}P(SiMe_3)_2]\}_2$ was prepared similarly to the method of Steigerwald and co-workers.[10] PH_3 was used as received from Matheson. *Caution! Phosphine (PH_3) is highly toxic and must be handled in accordance with proper safety measures.*[38] *We used PH_3 from a lecture bottle by bubbling small amounts through reaction solutions in a well-ventilated hood, and by passing the effluent gas from the reaction solutions through aqueous sodium hypochlorite to destroy unreacted PH_3.*[38] The reagents $PhCO_2H$ (Fisher), PhSH (Aldrich), Et_2NH (Fisher), and Et_3N (Aldrich) were used as received. Indium metal shot and P_4 (white phosphorus) were used as received from Strem. Methanol and *t*-BuOH were dried over Mg activated by I_2, and distilled. Hexane, toluene, mesitylene, and THF were distilled from sodium−benzophenone ketyl. 1,3-Diisopropylbenzene was sequentially washed with concentrated H_2SO_4, deionized H_2O, dilute NaOH, and deionized H_2O, then sequentially dried over CaH_2 and KOH (s), and finally sparged with N_2. NMR solvents were sparged with N_2 and stored over type 4A sieves.

Melting points were measured under N_2. C, H, and N analyses were performed by Oneida Research Services, Whitesboro, NY. NMR spectra were recorded at a field corresponding to 300 MHz for ^1H. XRD patterns were recorded on a Rigaku DmaxA diffractometer using Cu Kα radiation (λ = 1.541 845 Å) and Materials Data Inc. (MDI) software. Experimental powder patterns were compared to the JCPDS reference patterns for InP (32-0452) and In metal (05-0642). Coherence lengths (crystalline-domain dimension) were estimated by the JADE X-ray powder data processing program, which uses the Scherrer formula. Kα2 features and background counts were stripped from the data, and fwhm values were determined by peak integration; a term correcting for instrumental broadening was included. The reported coherence lengths are averages of the values obtained from the three major InP reflections, or the 100% reflection of In.

Specimens for TEM analyses were prepared from pyridine suspensions of the product powders generated in an ultrasonic cleaning bath. A few drops of the suspensions were applied to the TEM substrates (placed on absorbent tissues). The substrates were holey, amorphous carbon films on copper grids. Some specimens were loaded into the sample probe in a N_2-atmosphere glovebox and sealed by an air-tight protective sleeve with an O-ring fitting. The probe was then inserted into the microscope port through a N_2-filled glovebag. The analyses were performed on a JEOL 2000 FX transmission electron microscope, fitted with a Noran Voyager X-ray spectrometer for energy-dispersive spectroscopic (EDS) elemental analyses.

Formation of InP by Methanolysis of $\{t\text{-}Bu_2In[\mu\text{-}P(SiMe_3)_2]\}_2$ (1). Compound **1** (1.10 g, 1.35 mmol) was suspended in toluene (30 mL), and MeOH (0.22 mL, 0.17 g, 5.4 mmol) was added at room temperature, resulting in a clear colorless solution within 3−4 min. Stirring was continued for 10 h whereupon the color changed to yellow orange. The reaction mixture was then refluxed for 24 h in a heating mantle. The color of the solution changed to dark orange within the first 10 min at reflux, and then polycrystalline InP precipitated slowly as a black solid. The mixture was allowed to cool, and the InP was collected by filtration, washed with hexane (2 × 10 mL), and dried in vacuo (yield 0.31 g, theoretical InP weight yield 0.40 g). Anal. Found: C, 1.02; H, 0.08. EDS (atom %): calcd for InP, In, 50; P, 50; found, In, 46; P, 49.

The XRD pattern of the black solid indicated an average InP crystallite coherence length of ca. 11 nm (Figure 1a). A small amount of indium metal was also detected. The coherence lengths of InP varied from 9 to 16 nm and the In coherence lengths varied from 29 to 71 nm with decreasing stirring time prior to refluxing.

Preparation of $[t\text{-}Bu_2In(\mu\text{-}OMe)]_2$ (2) by Methanolysis of 1. Compound **1** (0.66 g, 0.81 mmol) was suspended in hexane (5 mL). MeOH (66 μL, 0.052 g, 1.62 mmol) was added at room temperature with stirring, whereupon a homogeneous solution formed in 2 min. The solution was stirred at room temperature for 2 min and then stored at −75 °C for 10 h. Colorless crystals of **2** were deposited. The supernatant was removed by cannula, and the crystals of **2** were dried in vacuo (yield 0.25 g, 0.48 mmol, 59%). Mp: 121 −122 °C. Anal. Calcd for $C_{18}H_{42}O_2In_2$: C, 41.56; H, 8.14. Found: C, 41.03; H, 8.04. ^1H NMR (δ, benzene-d_6): 3.46 (s, 6 H, OMe), 1.39 (s, 36 H, t-Bu). IR (cm^{-1}, KBr): 2945 s, 2925 s, 2829 vs, 2761 w, 2703 w, 1465 vs, 1360 m, 1248 w, 1191 w, 1158 m, 1051 s, 1012 m, 836 w, 808 s, 625 w, 439 s.

Preparation of $[t\text{-}Bu_2In(\mu\text{-}PHSiMe_3)]_2$ (3) by Methanolysis of 1. Compound **1** (1.47 g, 1.81 mmol) was suspended in hexane (4 mL) at room temperature. MeOH (147 μL, 0.116 g, 3.62 mmol) was added at room temperature with stirring, whereupon a homogeneous solution formed in 2 min. The solution was stirred at room temperature for 3 h and then stored at −23 °C for 5 h. Colorless crystals of **3** were deposited. The supernatant liquid was removed by cannula, and the crystals were dried under reduced pressure. A second crop of **3** was obtained similarly after reducing the volume of the supernatant to 2 mL (total yield 0.97 g, 1.45 mmol, 80%). Dec pt: ≥110 °C (slow decomposition). Anal. Calcd for $C_{22}H_{56}P_2Si_2In_2$: C, 39.53; H, 8.44. Found: C, 39.74; H, 8.53.

Compound **3** was soluble in THF and hydrocarbon solvents. ^1H NMR (δ, toluene-d_8): 1.53 (d, $^1J_{H-P}$ = 231 Hz, 0.50 × 2 H, P*H* of cis or trans isomer), 1.45 (d, $^1J_{H-P}$ = 234 Hz, 0.50 × 2 H, P*H* of trans or cis isomer), 1.45 (s, 0.50 × 18 H, *t*-Bu of cis isomer), 1.41 (s, 0.50 × 36 H, *t*-Bu of trans isomer), 1.37 (s, 0.50 × 18 H, *t*-Bu of cis isomer), 0.30−0.27 (complex m, 36 H, $SiMe_3$ of trans and cis isomers). ^{31}P NMR (ppm, toluene-d_8): −237.0 (dd, $^1J_{P-H}$ = 163 Hz, $^3J_{P-H}$ = 71 Hz, *P*$HSiMe_3$ of cis or trans isomer), −239.5 (dd, $^1J_{P-H}$ = 164 Hz, $^3J_{P-H}$ = 71 Hz, *P*$HSiMe_3$ of trans or cis isomer). IR (cm^{-1}, KBr): 2942 m, 2920 m, 2826 m, 2757 w, 2700 w, ν_{P-H} 2301 w, 1461 m, 1360 m, ν_{Si-Me} 1248 s, 1154 m, 1012 m, ν_{Si-Me} 839 vs, 807 s, 771 m, 700 w, 625 vs, 436 vs.

Preparation of $[t\text{-}Bu_2In(\mu\text{-}PH_2)]_3$ (4) by Methanolysis of 3. MeOH (61 μL, 0.048 g, 1.5 mmol) was added to a toluene (2 mL) solution of **3** (0.50 g, 0.75 mmol) at room temperature. The reaction mixture was stirred for 3 h at room temperature, and then stored at −23 °C whereupon pale yellow crystals of **4** deposited in 15 h. The supernatant was removed by cannula, and the crystals were dried (yield 0.21 g, 0.27 mmol, 53%). Dec pt: 115−120 °C. The thermal instability of **4** precluded elemental analysis.

Compound **4** was soluble in hydrocarbons, but decomposition began immediately in solutions prepared at room temperature as evidenced by ^1H NMR. ^1H NMR (δ, benzene-d_6): 1.60 −1.30 (br m, 0.77 × 54 H, *t*-Bu), 1.34 (s, 0.23 × 54 H, *t*-Bu). Resonances for the PH_2 protons

(34) Stoll, S. L.; Bott, S. G.; Barron, A. R. *J. Chem. Soc., Dalton Trans.*, in press.
(35) Leman, J. T.; Barron, A. R. *Organometallics* **1989**, *8*, 2214.
(36) Bürger, H.; Goetze, U. *J. Organomet. Chem.* **1968**, *12*, 451.
(37) Goel, S. C.; Cha, D.; Chiang, M. Y.; Buhro, W. E. To be published.
(38) (a) Fluck, E. *Fortschr. Chem. Forsch.* **1973**, *35*, 1. (b) Braker, W.; Mossman, A. L. *Effects of Exposure to Toxic Gases - First Aid and Medical Treatment*; Matheson Gas Products: East Rutherford, NJ, 1970; pp 37−38, 86−96.

Table 2. Crystallographic Data for **2**−**4**

	2	**3**	**4**
chemical formula	$C_{18}H_{42}In_2O_2$	$C_{22}H_{56}Si_2P_2In_2$	$C_{24}H_{54}P_3In_3$
color	colorless	colorless	pale yellow
a (Å)	14.598(6)	8.643(1)	11.327(3)
b (Å)	10.814(5)	11.181(2)	
c (Å)	9.748(3)	18.237(2)	16.962(7)
β (deg)	129.11(2)	94.19(1)	
V (Å^3)	1194.0(8)	1757.7(4)	1884.6(15)
Z	2	2	2
formula weight	520.2	668.4	780.0
space group	*C*2/*m*	$P2_1/n$	$P\bar{6}2m$
T (°C)	22	22	-100
λ (Å)	0.710 73	0.710 73	0.710 73
ρ_{calcd} (g/cm^3)	1.447	1.263	1.375
μ (cm^{-1})	19.36	14.56	19.28
$R(F_o)^a$	0.0132	0.0293	0.0582
$R_w(F_o)^b$	0.0148	0.0452	0.0792
GOF	1.01	0.80	0.98

^{a} $R(F_o) = \Sigma||F_o| - |F_c||/\Sigma|F_o|$. ^{b} $R_w(F_o) = (\Sigma_w||F_o| - |F_c||^2/\Sigma w|F_o|^2)^{1/2}$; $w = [\sigma^2(F_o) + g(F_o)^2]^{-1}$.

could not be assigned with certainty. Resonances for isobutane (*t*-BuH), a primary decomposition product, were observed in every spectrum of isolated **4**: 0.85 (d, $^1J_{H-H} = 6.7$ Hz, *t*-Bu of isobutane). $^{31}P\{H\}$ NMR (ppm, benzene-d_6): −271.4 (s, PH_2). The proton-coupled ^{31}P NMR spectrum is shown in Figure 6.

Solution-Phase Decomposition of [*t*-Bu$_2$In(*μ*-PH$_2$)]$_3$ (4) at 111 °C. Compound **4** was generated *in situ* as follows. A solution of *t*-Bu_3In (0.372 g, 0.001 30 mmol) in toluene (15 mL) was prepared at room temperature. Excess PH_3 (g) was then bubbled into the solution. (In separate experiments the complete conversion of *t*-Bu_3In to **4** was confirmed by NMR monitoring.) The excess PH_3 was removed by sparging the solution with N_2, and then the solution was refluxed for 24 h in a heating mantle to yield a dark brown-black insoluble solid, which was collected by filtration, washed with hexane, and dried in vacuo (yield 0.192 g). Anal. Calcd for $[(t\text{-Bu})_{0.30}InPH_{0.30}]$: C, 8.90; H, 1.87. Found: C, 8.90; H, 1.44.

The XRD pattern for the solid contained both broadened (major) and sharper (minor) components corresponding to InP. Figure 1b shows the pattern for a sample prepared by this procedure.

MeOH-Catalyzed Decomposition of [*t*-Bu$_2$In(*μ*-PH$_2$)]$_3$ (4) at 111 °C. Compound **4** was generated *in situ* in toluene from *t*-Bu_3In (0.370 g, 1.29 mmol) and PH_3 as described above. MeOH (5.5 *μ*L, 0.0044 g, 0.14 mmol) was added, and the reaction mixture was stirred at room temperature for 12 h. The mixture was then refluxed for 24 h in a heating mantle, whereupon InP was precipitated as a black solid. The product was collected by filtration, washed with hexane, and dried in vacuo (yield 0.132 g, theoretical InP weight yield 0.19 g). Anal. Found: C, 1.04; H, 0.10.

The XRD pattern of the black solid indicated an average InP crystallite coherence length of ca. 10 nm (Figure 1c). A small amount of indium metal was also detected.

General Procedure for Formation of InP from Catalyzed Reactions of *t*-Bu$_3$In and PH$_3$. Compound **4** was generated *in situ* as described above, in either toluene or 1,3-diisopropylbenzene. The normal reaction used 0.370 g (1.29 mmol) of *t*-Bu_3In and 15.0 mL of solvent; moderate variations in scale and concentration did not appear to alter the results. A protic catalyst (or potential catalyst; see Table 1) was then added in 10−11 mol % relative to *t*-Bu_3In. The resulting solution was stirred for 12 h at room temperature prior to heating; moderate variations in this interval did not appear to alter the results. The reaction mixture was then refluxed for approximately 24 h. Heat was applied to some reactions by a heating mantle (with a consistent variac setting), and to others by an oil bath. Yields, crystalline coherence lengths, and elemental analyses are summarized in Table 1.

(39) *International Tables for X-ray Crystallography*; Hahn, T., Ed.; Kynoch Press: Birmingham, England, 1974; Vol. IV, pp 99, 149.

Formation of InP by Reaction of Dispersed Indium and P$_4$. A stock solution of P_4 (0.862 g, 6.96 mmol) in mesitylene (50 mL) was prepared at room temperature and stirred overnight. Indium shot (1.015 g, 8.840 mmol) was melted in refluxing mesitylene (50 mL, 164 °C) and then dispersed by high-intensity ultrasonic irradiation with a titanium immersion horn, forming a suspension of micrometer-sized particles. Ultrasonic irradiation was then discontinued, and a portion of the P_4 solution (16.0 mL) was injected rapidly into the hot indium dispersion, resulting in a near instantaneous darkening of the light-gray color. The mixture was allowed to cool and settle, and the solid component was collected by filtration, washed with hexane, and dried in vacuo to give a dark-gray powder.

The XRD pattern for the solid contained only reflections for In and InP; the data indicated an average coherence length of 59 nm for InP.

The experiment was repeated in the manner described above, except in refluxing toluene (111 °C) instead of refluxing mesitylene as the reaction medium. The In dispersion used was first sonicated in hot mesitylene, cooled, washed, dried, and added to toluene. Analysis by XRD confirmed that no crystalline InP was formed.

Crystallographic Procedures. Suitable crystals of **2**−**4** for diffraction analysis were obtained directly from their respective reaction mixtures at −23 °C. Crystals were mounted in thin-wall glass capillaries in an inert-atmosphere glovebox. Intensity data were collected on a Siemens R3m/V diffractometer.

Crystallographic calculations were done with the Siemens SHELXTL PLUS program package. Crystal data are summarized in Table 2. Neutral-atom scattering factors were used.[39] All structures were solved by direct methods. The space groups assigned on the basis of systematic absences were *C*2*m* for **2** and $P2_1/n$ for **3**. Five space groups were possible for **4** (i.e., *P*622, no. 199; *P*6*mm*, no. 183; $P\bar{6}2m$, no. 189; *Pm*2, no. 187; and *P*6/*mmm*, no. 191); successful refinement confirmed the choice of space group $P\bar{6}2m$ (no. 189). Refinement results for each are described in the Supporting Information. Except for **4** (see below), all non-hydrogen atoms were refined anisotropically. All hydrogen atoms were placed in calculated positions ($d_{C-H} = 0.96$ Å) and included in the final structure factor calculations by using a riding model, except for H(1) in compound **3** for which positions and *U* were refined.

In **4**, the asymmetric unit contained two trimeric units, one of which exhibited disordered Me groups on the *t*-Bu substituents. The disordered carbon atoms were fixed at their found positions, and their isotropic thermal parameters were refined. The In and P atoms for the disordered unit were refined anisotropically. Hydrogen atoms on the disordered moiety were omitted. Final positional parameters are given in the Supporting Information.

Acknowledgment. We are grateful to Dr. Douglas M. Ho (Princeton University) for crucial assistance with the crystal structure of **4** and to Professor Andrew R. Barron (Rice University) for sharing results prior to publication. Funding was provided by an NSF Presidential Young Investigator Award (Grant CHE-9158369), the Eastman Kodak Co., the Emerson Electric Co., the Exxon Education Foundation, and the Monsanto Co. K.M.H. was supported by a Department of Education GANN grant. Washington University's X-ray Crystallography Facility was funded by the NSF Chemical Instrumentation Program (Grant CHE-8811456). The Washington University High-Resolution NMR Service Facility was funded in part by NIH Biomedical Research-Support Shared-Instrument Grants RR-02004, RR-05018, and RR-07155, and a gift from the Monsanto Co.

Supporting Information Available: Tables listing details of the crystallographic data collection, atomic coordinates, bond distances, calculated hydrogen atom parameters, and anisotropic thermal parameters (and text giving additional experimental details (27 pages). See any current masthead page for ordering and Internet access instructions.

JA9640859